Switch and Act of a Cascaded Shunt Active Power Filter for Aircraft Electric Power System

K. Venkatesh[1], R.S. Sai Praveen Kumar[2]
[1, 2] SVPCET,PUTTUR.

Abstract- *With the progress of "more electric aircraft," introducing active power filter (APF) technology into the aircraft power system to improve its quality and reliability catches growing inter- est. In this paper, based on the analysis and modeling of the shunt APF with close-loop control, a feedforward compensation path of load current is proposed to improve the dynamic performance of the APF. The two H-bridge cascaded inverter is selected for the aeronautical APF (AAPF). Justifications for topology choosing and corresponding system control method are given. Furthermore, the global framework and operation principle of the proposed AAPF are presented in detail. A prototype with the load power of 7.2 kVA is built and tested in the laboratory. Experimental results verify the feasibility of the proposed AAPF and the high perfor- mance of the control strategy during steady-state and dynamic operations.*

Keywords- Aeronautical active power filter (APF) (AAPF), cascaded multilevel inverter, close-loop control, feedforward of fundamental load current

I. INTRODUCTION

THE increasing use of electrical power in place of hy- draulic, pneumatic, and mechanical power is demanding more advanced aircraft power systems. The concept of the "all-electric aircraft" and the "more electric aircraft" (MEA) have been introduced to overcome some of the drawbacks found in conventional architectures and bring more attractive advantages, such as improved fuel consumption and lower maintenance and operation costs . This implies an increase of the electrical load and power electronic equipment, higher consumption of electrical energy, more demand for generated power, power quality, and stability problems.

Fig. 1 illustrates the next-generation electrical power sys- tem (EPS) of MEA. In the variable-speed variable-frequency (VSVF)-based EPS, the "constant speed drive" is moved. Har- monic current compensation by means of active power filter (APF) is a well-known effective solution for the reduction of current distortion and for power quality improvement in electrical systems. The shunt compensator behaves as a controlled current source that can draw any chosen current ref- erences which is usually the harmonic components of the load currents . Meanwhile, more and more APFs are applied not only in harmonic current and reactive power compensation but also in the neutral line current compensation, harmonic damping application, and power flow control. As Fig. 1 shows, in the aircraft EPS, the APF could be installed in the source side (such as the aircraft generator) or near the load side, and it could even be integrated into the load-front converter (such as the input stage converter of variable-speed drives).

Introducing APF technology to resolve the power quality issues of the aircraft EPS catches increasing attention. Several papers have been published about the APF's application in the aircraft EPS since 2005. In Ganthony and Bingham pro- posed an integrated series active filter for aerospace flight control surface actuation. Simulation results based on Matlab are given as well as the hardware platform picture. In Lavopa et al. proposed an estimation method of fundamental frequency and harmonics for APF applications in aircraft sys- tems, and its transaction version. Good harmonic real- time detection performance is achieved from both simulation and experimental waveforms. In Odavic et al. proposed a current control strategy for shunt APF in aircraft power networks. A predictive controller with a genetic algorithm and multilevel converters are applied. In order to compensate the inherent delay of digital control systems, Biagini et al in- vestigated the development of an improved deadbeat controlled shunt APF for aerospace applications working in an aircraft power system with a supply frequency of 400 Hz. In a multiresolution control strategy is proposed for the DSP con- trolled shunt APF to reduce real-time computational require- ments. However, the system dynamic performance from the given experimental result is not improved. In a shunt APF using perfect harmonic cancellation is studied. The harmonic filtering performance of the APF in both the conventional and the advanced aircraft EPS is presented with Matlab simulation results. In based on the given structure and modeling of the advanced aircraft EPS, performance characteristics of the EPS without and with APF are compared. The power-quality char- acteristics of both the conventional and the advanced aircraft EPS with APF are shown to be in compliance with the popular electrical standards, i.e.,.

In this paper, a high-performance aircraft APF is proposed. Differently from traditional open-loop control strategy, the proposed aeronautical APF (AAPF) works in a close-loop way. Good power quality of the EPS is achieved by using the novel AAPF. Furthermore, in order to improve the dynamic perfor- mance of the load response, a feedforward path of the load

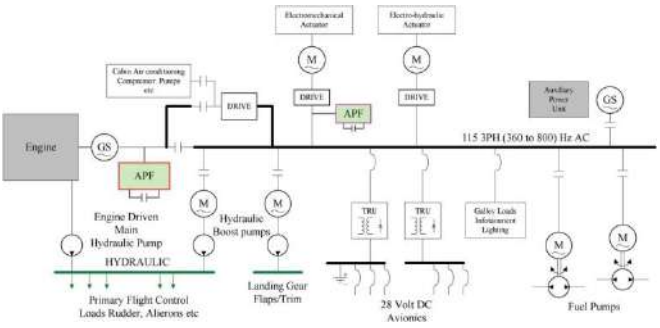

Fig. 1. Next-generation electrical system of MEA.

current is added. Based on the modeling and analysis of the close-loop system, the operation principle of the feedforward compensation path is revealed. Meanwhile, the control method of the cascaded-inverter-based AAPF is proposed. The op- eration principle containing the overall voltage control and voltage-balance control is given. Simulation results under dif- ferent fundamental frequencies and load conditions are given. In order to verify the aforementioned analysis and compen- sation performance of the proposed AAPF, an aircraft APF system with a 7.2-kVA load power is built and tested in the lab- oratory. Experimental waveforms in different load conditions indicate the good performance of the AAPF.

II. CLOSE-LOOP CONTROL STRATEGY AND ITS FEEDFORWARD COMPENSATION

A. Close-Loop Control Strategy

In the traditional control of APF, the current reference is usu- ally the harmonic and reactive components of the load currents. However, the approach, essentially based on feedforward open- loop control, is sensitive to the parameter mismatches and relies on the ability to accurately predict the voltage-source inverter current reference and its control performance.

In the close-loop control, detection and control target is the source current. In the aircraft EPS, the fundamental frequency is much higher than 50-Hz power system. Furthermore, measure errors, analog to digital conversion time, digital delay, and other nonideal factors will deteriorate the open-loop compensation effect to a worse degree. As we known, feedback control has the following merits: It could reduce the transfer function from disturbances to the output, and it causes the transfer function from the reference input to the output to be insensitive to variations in the gains in the forward path. Therefore, compared with open-loop control, close-loop control is more suitable for the aeronautical application.

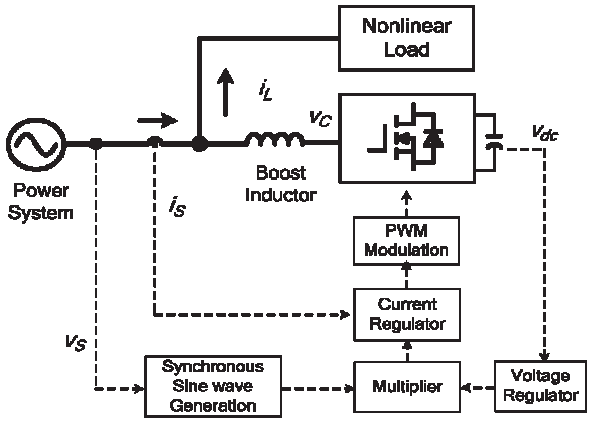

Fig. 2. Control diagram of source current direct control.

B. Source Current Direct Control

In this paper, the close-loop control named as source current direct control is applied as the main control strategy of the proposed AAPF. The source current direct control is proposed in by Wu and Jou. The basic system diagram of the close- loop control scheme is given in Fig. 2. This control strategy operates as follows: The dc-link voltage is sent to the voltage regulator, and the output of the regulator is sent to the multiplier as well as a synchronous sine wave which is detected from the phase voltage. The output of the multiplier is sent to the current regulator, being the source current reference. The output of the current regulator will be sent to the modulator to generate the pulsewidth modulation waveforms. Fig. 3 gives the equiv- alent control model of this compensation strategy. As shown in Fig. 3, the source current reference of the source current direct control comes from the variation of the dc-link voltage. Here, ttv(s) corresponds to the transfer function of the voltage controller; Kf is the dc-link voltage detection coefficient.

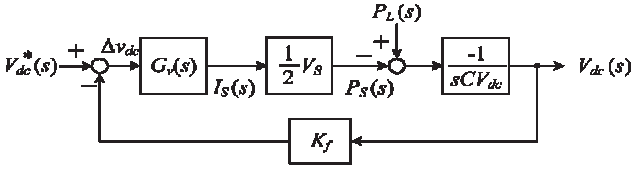

Fig. 3. Model for active power analysis.

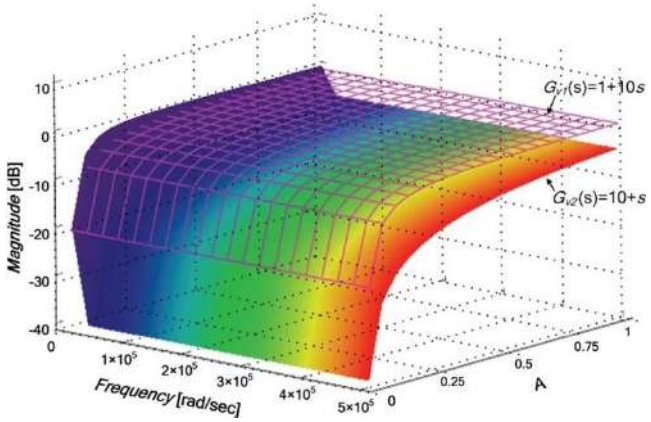

Fig. 4. Bode diagram of transfer function HiL(s).

C. Load Current Feedforward Compensation

As Fig. 3 illustrates, load power PL(s) works as a distur- bance factor on the APF system. The transfer function between PL(s) and ΔVdc(s) is

$$\Phi_{en}(s)=\frac{\Delta V_{dc}(s)}{P_L(s)}=\frac{\frac{1}{sCV_{dc}}K_f}{1+tt_v(s)\cdot\frac{V_S}{2}\cdot\frac{1}{sCV_{dc}}K_f} \quad (1)$$

The transfer function between $I_L(s)$ and $I_S^*(s)$ is

$$\frac{I_S^*(s)}{I_L(s)}=\frac{\Delta V_{dc}(s)tt_v(s)}{I_L(s)\frac{V_S}{2}}=\frac{A\cdot tt_v(s)}{s+A\cdot tt_v(s)} \quad (2)$$

where A = VsKf /(2CVdc) $H_{iL}(s)_{f=50}$ shows the dynamic speed of the current refer- ence responding to the load power's change at fundamental fre- quency. Generally speaking, high dynamic respond is required for an APF system, meaning that a higher value of $H_{iL}(s)_{f=50}$ is desired. However, $H_{iL}(s)$ is sensitive to many other factors, i.e., voltage controller, line voltage, dc-link voltage, dc-link capacitor, and voltage detection coefficient. Fig. 4 shows the bode diagram of $H_{iL}(s)$ in different voltage controller and coefficient A. For an APF system applied in a 220-V/50-Hz application, coefficient A corresponds to 0.14 when the dc-link voltage is 800 V, dc-link voltage detection coefficient K_f is 0.005, and the dc-link capacitor is 6800 μF. It is hard to design a voltage controller to derive a high value for $H_{iL}(s)_{f=50}$ at 50 Hz in such a low value of A. In the aircraft EPS, the phase voltage is only 115 V, leading A to be 0.2 when the dc-link voltage is 600 V, dc-link voltage detection coefficient K_f is

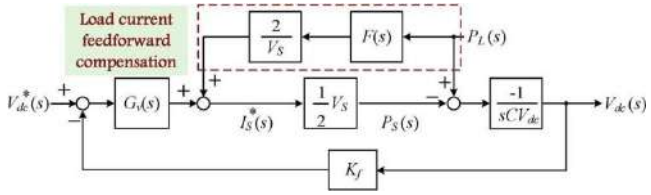

Fig. 5. Disturbance compensation-based lose-loop control.

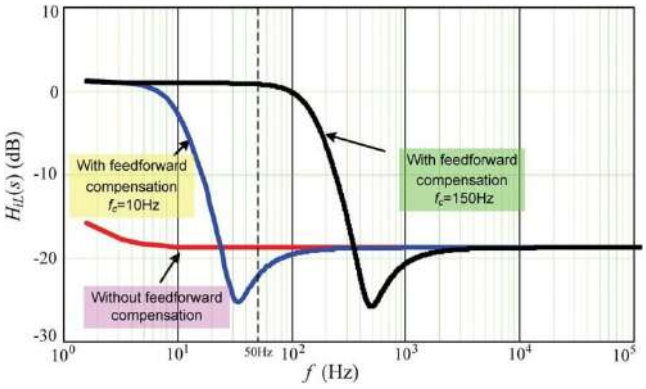

Fig. 6. Amplitude-frequency characteristic of HiL(s).

0.005, and the dc-link capacitor is 3300 µF. It means that poor dynamic respond is derived in both applications.

In order to improve the dynamic speed responding to the load's change, A feedforward compensation path is added to weaken the disturbance effect of the load current, as shown in Fig. 5. Here, F (s) is the transfer function of the low-pass filter (LPF) which extracts the fundamental components of the load currents

$$F(s)=\frac{\omega_0}{s+\omega_0} \quad (3)$$

Here, $\omega_0 = 2\pi f_c$ is the cutoff angular frequency of the LPF.

After the fundamental of the load current is feedforward, the

$$H_{iL}(s)=\frac{A\cdot tt_v(s)}{s+A\cdot tt_v(s)}+\frac{\omega_0^2}{s^2+\sqrt{2}\omega_0 s+\omega_0^2} \quad (4)$$

Fig. 6 shows the bode diagram of HiL(s) with feedforward compensation and different cutoff frequencies. After the load current is feedforward, the magnitude of HiL(s) f=50 gets increased. However, the selection of fc plays an important role to HiL(s); usually, fc should be larger than the fundamental frequency.

III. CONTROL METHOD OF THE CASCADED-INVERTER-BASED AAPF

A. Discussion and Demonstration on the Power Stage of AAPF

A shunt APF acts as a controlled harmonic current source, injecting current which is inverse equivalent to the load har- monic. In the 400-Hz aircraft EPS, frequencies of the 11th and 13th harmonics reach as high as 4.4 and 5.2 kHz. How to draw a high-frequency harmonic current accurately is a key issue of developing AAPF.

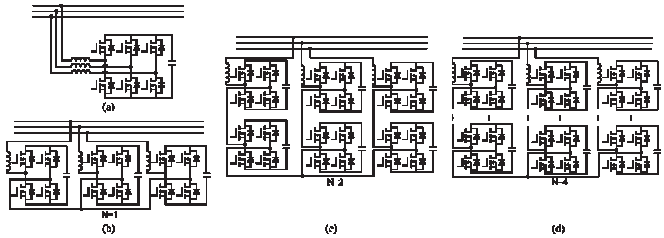

Fig. 7. Four possible solutions of AAPF. (a) Three-leg-inverter-based APF. (b) H-bridge-based APF. (c) Two H-bridge cascaded APF. (d) Four H-bridge cascaded APF.

TABLE I
PARAMETERS OF FOUR POSSIBLE AAPF SOLUTIONS

Solution	Dc-link voltage (V)	Power Device	Switching Frequency (kHz)
Three-leg inverter based APF	400	IRFP26N60L	60
			120
			240
H-bridge based APF	300	IRFP23N50L	30
			60
			120
Two H-bridge cascaded APF	150	IRFP254N	15
			30
			60
Four H-bridge cascaded APF	75	IRFP23N15D	7.5
			15
			30

Fig. 7 shows four possible solutions of AAPF: the three- leg-inverter-based APF, the H-bridge-based APF, the two H-bridge cascaded APF, and the four H-bridge cascaded APF. Comparative study of these solutions is taken as follows.

For the first solution, in order to achieve good current track- ing performance in 400-Hz system, the switching frequencies of AAPF are selected as 60, 120, and 240 kHz, and the dc-link voltage is adopted as 400 V.

For the second solution, considering the "double equivalent switching frequency effect" of the carrier phase shift (CPS) PWM modulation, the switching frequencies of AAPF are selected as 30, 60, and 120 kHz, and the dc-link voltage is adopted as 300 V. Meanwhile, the same equivalent switching fre- quency means almost the same current tracking performance and almost the same bandwidth of AAPF. The switching frequen- cies and dc-link voltage of the other two solutions are given in Table I. The power switches in Table I are all from International Rectifier (IR) Corporations with the current rating near 24 A.

The switching losses and conductive losses of the power MOSFET could be evaluated by using the switching loss es-timation method used in as follows:

$$P_{SW} = \frac{1}{2} I_D V_D (t_{OFF} + t_{ON}) f_{sw} + \frac{1}{2} C_{OSS} V_D^2 f_{sw} \quad (5)$$

$$P_{con} = I_{RMS}^2 R_{ds(on)} D + V_{DF} I_D (1 - D). \quad (6)$$

Here, PSW and Pcon correspond to switching loss and con- ductive loss, and ID, VD, and fsw are the drain current, bus voltage, and switching frequency, while tON and tOF F are the power MOSFET turn-on and turnoff times, respectively. COSSRds(on) are the output capacitance and the on-resistance of the power MOSFET while VDF is the forward voltage drop of the reverse parallel diode of the power MOSFET.

Power loss distributions of the four different AAPF solutions are given in Fig. 8. As Fig. 8 shows, the following conclusion could be made.

1) Compared with the last two solutions, switching power loss plays important roles for the first two solutions. Unnegligible switching power losses make the first two solutions less competitive when the switching frequency increases.

2) Negligible switching power losses in the last two solu- tions make the total power losses smaller in a wide range of switching frequency. Meanwhile, power losses of the last two solutions are nearly in the same level.

On the other hand, the "dead-time effect" deteriorates the current tracking performance of APF, particularly in the high switching frequency application. For the multilevel cascaded converter with CPS PWM modulation, the "dead-time effect" could be attenuated in a large degree by using a relatively low switching frequency.

In this paper, the two H-bridge cascaded APF is selected as the power stage configuration of the AAPF, both for the accepted small power loss and reliability (as shown in Fig. 9). The switching frequency is selected as 30 kHz, so the ac voltage of each cluster becomes a five-level line-to- neutral PWM waveform with the lowest harmonic sideband centered at 120 kHz (= 30 kHz 2 2). Maintenance of the voltage balance of the capacitors is critical to the safe operation of the H-bridge-based AAPF. The voltage-balance control of the floating dc capacitors can be divided into the following:

1) clustered overall control;
2) balancing control.

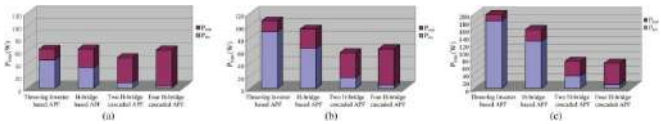

Fig. 8. Power losses of different possible AAPF solutions. (a) With the equivalent switching frequency feq of 60 kHz. (b) With the equivalent switching frequency feq of 120 kHz. (c) With the equivalent switching frequency feq of 240 kHz.

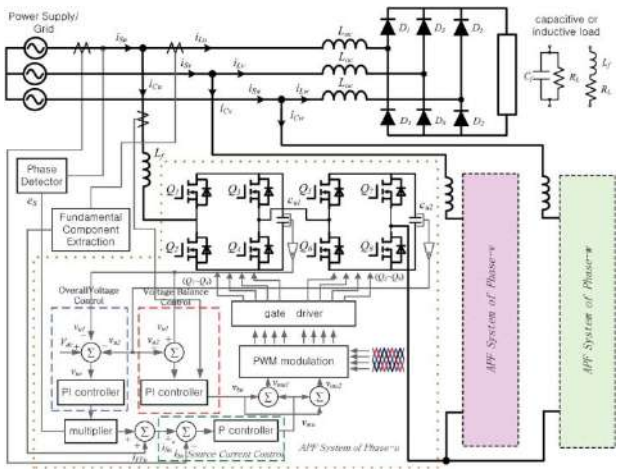

Fig. 9. System diagram of the proposed AAPF.

B. Clustered Overall Control

In the cluster overall voltage control loop, sums of the capacitor voltages in each cluster (for example: vu1 and vu2 for phase-u) are the control target. This cluster overall control yields the u-phase clustered overall voltage signal vou from the dc capacitor voltage reference vdc, the dc capacitor voltages of the u-phase cluster vu1, vu2, and the synchronous sine wave eSu (as shown in Fig. 10). Furthermore, this voltage control scheme could be expanded to the N H-bridge cascaded inverter topology. Here, N corresponds to the number of cascaded converter units.

One obvious advantage of this control scheme is that the final compensation performance would not get worse when one or more cascaded units stop working. The remaining cascaded

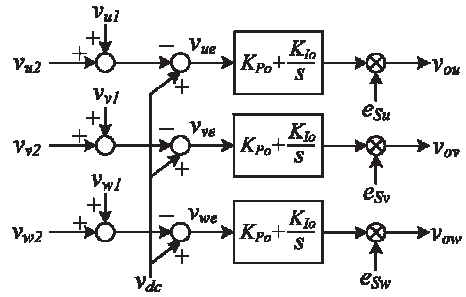

Fig. 10. Control diagram of the cluster overall control.

units would share the dc-link voltage of the fault one. This voltage control scheme can increase the fault toleration and reliability of the AAPF system.

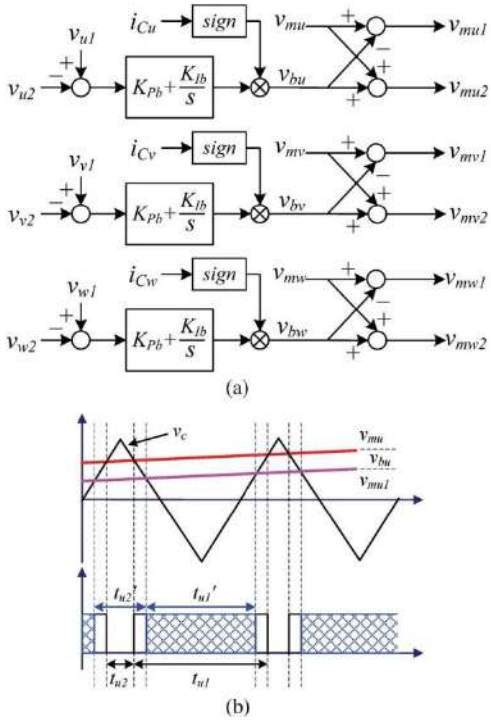

Fig. 11. Operation principle of voltage-balance control. (a) Control diagram. (b) Regulation procedure.

C. Balancing Control

As Fig. 11(a) shows, the balancing control yields a balance control signal vbn(n = u, v, w) to make the voltage of the capacitors in each cluster balanced. The individual balance control yields two modulation waves vmn1 and vmn2 from the origin modulation wave vm and the dc capacitor voltages of

each cluster vn1, vn2. In the CPS PWM modulation, PWM signals for Q1, Q2 and Q3, Q4 are modulated by vmn1, while PWM signals for Q5, Q6 and Q7, Q8 are modulated by vmn2.

The current direction and the switch combination define the charging or discharging of the each particular capacitor of the dc link. Depending on the current direction and needed charging or discharging process, the voltage signal vbu should be added or subtracted to/from the modulating signal. For the upper cascaded unit, the input power decreases when the duty cycles of Q1 and Q4 decrease, resulting in the dc-link voltage vu1 being reduced. Similarly, the dc-link voltage of the lower cascaded unit vu2 will get increased. The voltage balance is therefore achieved.

Take the phase-u cluster for example to show the regulation procedure of voltage-balance control [as shown in Fig. 11(b)]. In the steady state, the modulation wave of bridge 1 (composed of Q1 and Q2) is vmu, and the conduct times of Q1 and Q2 are tu1 and tu2, respectively. When the situation vu1 > vu2 happens, a positive balance control voltage signal vbu is obtained under the regulator's action. As Fig. 11(a) shows, the final modulation wave for Q1 and Q2 is the sum of vmu and vbu, which becomes vmu1 after regulation. Therefore,
the conduction times of Q1 and Q2 turn to be tJu1 and tJu2. As Fig. 11(b) illustrates, we could find that tJu1 < tu1 and tJu2 > tu2, which means that the duty cycle of Q1 decreased

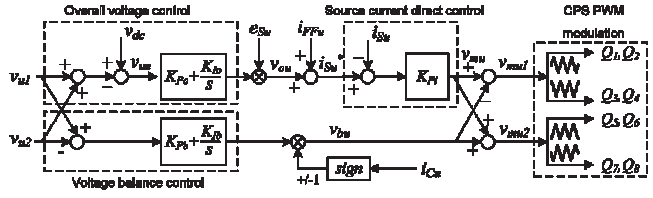

Fig. 12. Control diagram for phase-u of the proposed AAPF.

but the duty cycle of Q2 increased. Meanwhile, the duty cycle of Q3 increased, and the duty cycle of Q4 decreased.
The whole control diagram for phase-u of the proposed
AAPF is given in Fig. 12, which contains the overall voltage control, voltage-balance control, load current feedforward com- pensation, and source current direct control.

IV. SIMULATION RESULTS

In order to verify the compensation performance of the pro- posed AAPF, simulated waveforms using the "Simulink" soft- ware package of "Matlab" are given. The system power PL is set as PL = 7.2 kVA, and the dc-link voltage Vdc and the switch- ing frequency fSW are set as Vdc = 150 V and fSW = 25 kHz.

Fig. 13 shows the simulated waveforms for the 400-Hz EPS with inductive load. Nonlinear loads start to work at 0.2 s and are half unloaded at 0.25 s. As Fig. 13(a) indicates, compensa- tion voltage vCu is a five-level voltage, and three phase source currents get sinusoidal. In Fig. 13(b), the ac mains voltage is distorted, and a third-order (1.2-kHz) voltage harmonic corre- sponding to 20 V appears in the mains voltage.

After APF's working, the source current becomes nearly sinusoidal, and the total harmonic distortion (THD) of the source current is only 2.6%. The results show that good compensation performance is achieved by using the proposed AAPF under distorted ac mains. Fig. 14 shows the simulated waveforms for 400-Hz EPS with capacitive load. Nonlinear loads start to work at 0.2 s. Compared with the inductive load, five-level voltage appears more in the compensation voltage vCu. Fig. 14(b) indicates that
the voltage balancing of all the dc capacitors is achieved.

Fig. 15 shows the simulated waveforms for a variable- frequency EPS application, in which the fundamental frequency changes from 400 to 600 and 800 Hz in 1 and 1.01 s and back to 600 and 400 Hz in 1.02 and 1.03 s. All the waveforms indicate that the proposed AAPF could improve the source current in a wide range of the system frequency.
The THD values of the load current and source current in each condition are given in Table II.

V. IMPLEMENTATION

The proposed AAPF is tested with a laboratory setup com- posed of three single-phase two H-bridge cascaded voltage source inverters in a Y-connection [as shown in Fig. 16(a)]. The whole APF system consists of the power board, control board, drive board, signal board, and feedforward board. The signal board is in charge of the generation of the phase-shift triangle waves and the synchronous sine wave, while the feedforward board works to extract the fundamental components of the load

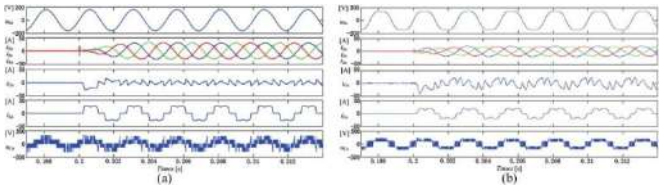

Fig. 13. Simulated waveforms for 400-Hz EPS application with inductive load. (a) With sinusoidal phase voltage. (b) With distorted phase voltage.

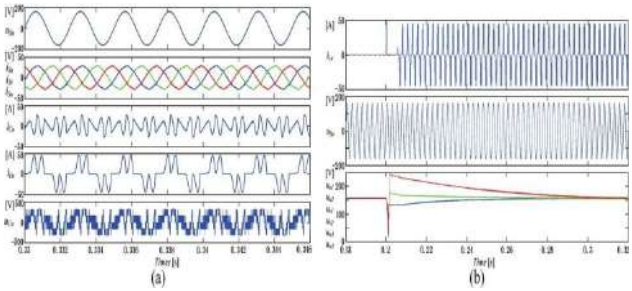

Fig. 14. Simulated waveforms for 400-Hz EPS application with capacitive load. (a) Key waveforms under loading. (b) DC capacitor voltage waveforms under loading.

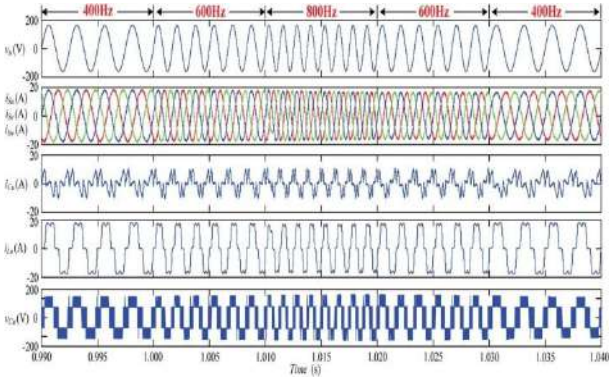

Fig. 15. Simulation waveforms of AAPF under variable-frequency EPS.

TABLE II
THD VALUES OF THE SOURCE CURRENT AND LOAD CURRENT WITH APF

Frequency		THD of i_L	THD of i_S
400Hz	inductive	28%	2.3%
	capacitive	79.7%	3.4%
	distorted ac mains	27.5%	2.6%
600Hz inductive		27.35%	2.8%
800Hz inductive		26.85%	3.6%

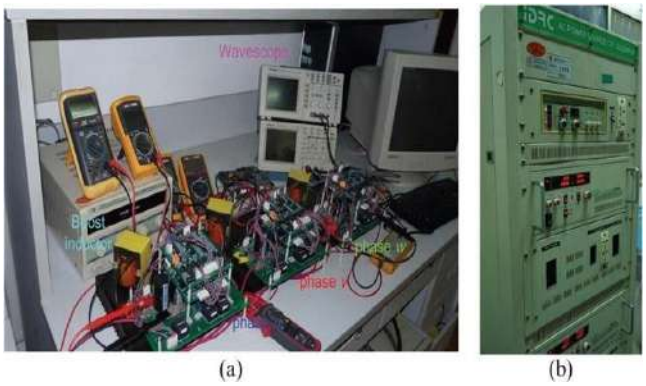

(a) (b)

Fig. 16. Picture of the laboratory setup where the AAPF is tested. (a) Three phase APF hardware platform. (b) 400-Hz ac power supply CIF-3030M3P.

TABLE III
PARAMETER AND CONSTANTS USED FOR THE LABORATORY SETUP

Parameter	Notation	Values used
Line voltage	V_S	115 V
Fundamental frequency	f_0	400 Hz
Load Power	P_L	7.2 kVA
Dc-link voltage of each inverter	V_{dc}	120 V
Switching frequency	f_{SW}	30 kHz
Switching device	Q	FQ24N60
Boost inductance in each inverter	L_f	600 µH
Dc capacitance	C_{dc}	680 µF
Inductance in the ac-side of the rectifier	L_{ac}	50 µH
Controller of dc-voltage loop	K_{Po}/K_{Io}	0.1/1
Controller of dc-voltage balance loop	K_{Pb}/K_{Ib}	0.3/0.5
Controller of source current control loop	K_{Pi}	5

current. Each single-phase active filtering module could work independently. The parameter values and controller gains are given in Table III.

The nonlinear load creating harmonic currents is a three- phase diode rectifier with a power of 7.2 kVA. The 400-Hz ac power is produced by an ac power supply CIF-3030M3P made by the IRDC Corporation [as shown in Fig. 16(b)].

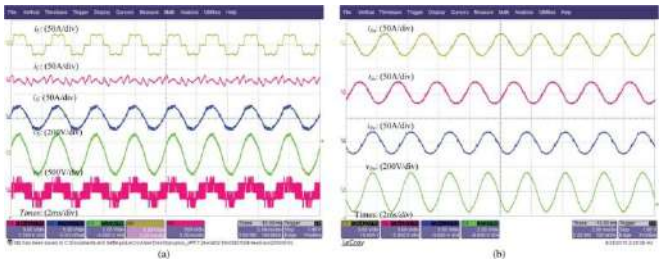

Fig. 17. Experimental waveforms of AAPF under inductive load power of 7.2 kW. (a) Waveforms of phase w. (b) Source current waveforms of each phase.

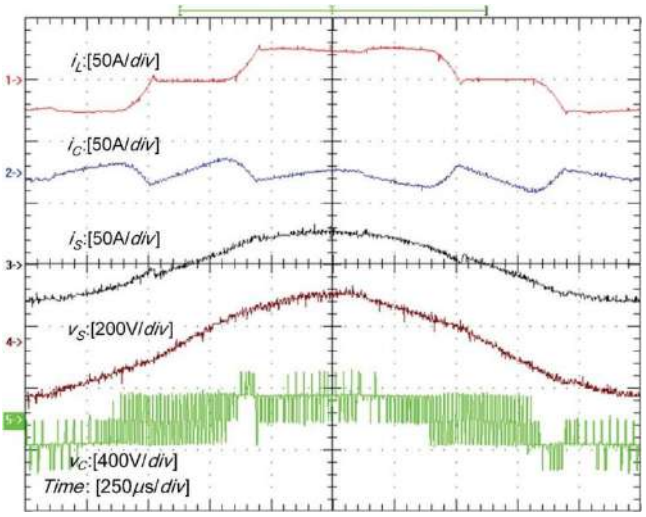

Fig. 18. Experimental waveforms of AAPF with a small time scale.

Fig. 17(a) shows the steady-state response of the proposed AAPF under the load power of 7.2 kW. From top to bottom, waveforms of the load current iL, compensation current iC , source current iS , source voltage vS , and compensation volt- age vC are given. Compensation voltage vC produced by the cascaded inverter is a five-level waveform. In Fig. 17(b), the source currents of three phases are nearly sinusoidal. Detailed experimental waveforms of phase-u with a small time scale are given in Fig. 18. As Fig. 19 illustrates, after APF's working, the THD of the source current is reduced from 34.06% to 3.37%.

Fig. 20 shows the dynamic response under the load changes with and without feedforward compensation. In Fig. 20(a), the feedforward compensation is unable, and the AAPF system responses in a slow dynamic speed. With the feedforward com- pensation, the dynamic response increases by a large degree, and the system goes to the stable state in less than two cycles [as shown in Fig. 20(b)]. Moreover, during the transient condition, the dc bus voltage goes stable much faster and has a smaller fluctuation when the feedforward compensation is added.

Fig. 21 shows the experimental waveforms of AAPF under capacitive load. Before AAPF's compensation, the load current

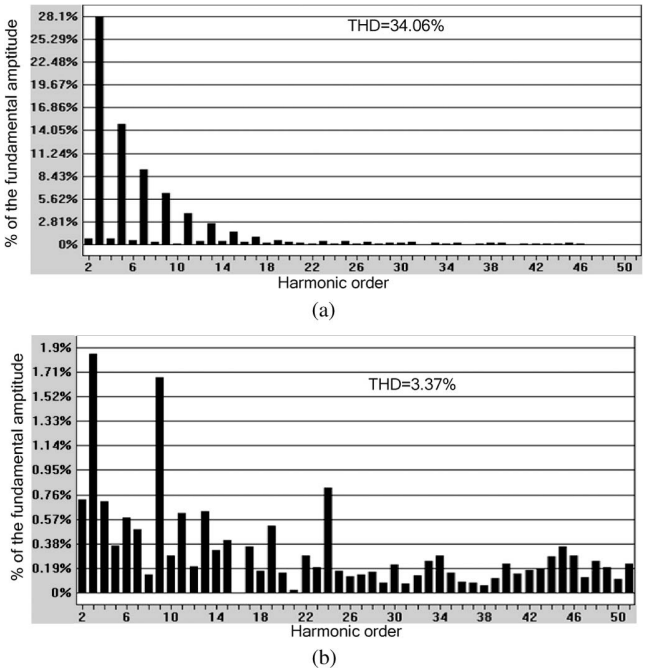

Fig. 19. Current THD. (a) Load current. (b) Source current.

is seriously distorted, and the peak value of the source current reaches a high level. It should be noted that, although the ac mains voltage is slightly distorted (with the THD of 5.2%), after AAPF's compensation, the source current gets improved.

VI. CONCLUSION

APF technology is a useful method to resolve the power quality issues of the modern aircraft EPS. In this paper, a load current feedforward compensation method for the source current direct control-based AAPF has been proposed. The corresponding system control strategy of the cascaded-inverter- based active filter system is shown. Experimental results from a laboratory setup with a load power of 7.2 kW are shown to con- firm the good compensation behavior for various kinds of non- linear load condition and the excellent dynamic performance

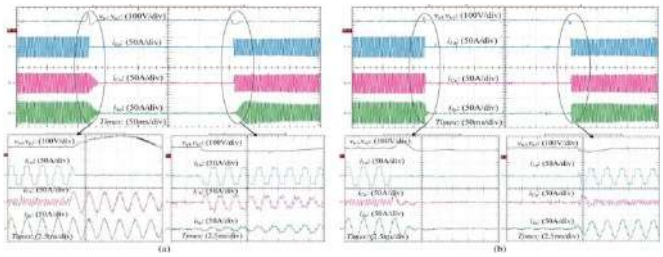

Fig. 20. Transient experimental waveforms when load power changes from full load to no load and no load to full load. (a) Without feedforward compensation.(b) With feedforward compensation.

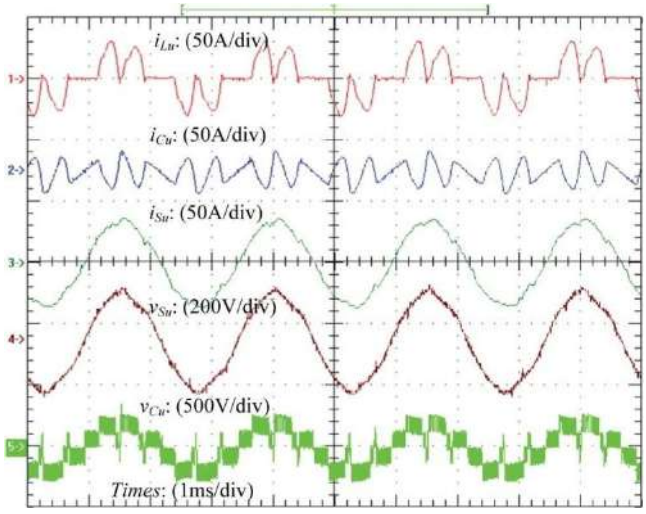

Fig. 21. Experimental waveforms of AAPF under capacitive load.

of the proposed control method. Because of the limitations of the hardware (800-Hz ac voltage source), experiments of the AAPF in variable-frequency applications have not been taken. More work in the plan will be taken in future.

REFERENCES

[1] J. A. Rosero, J. A. Ortega, E. Aldabas, and L. Romeral, "Moving towards a more electric aircraft," IEEE Aerosp. Electron. Syst. Mag., vol. 22, no. 3, pp. 3–9, Mar. 2007.

[2] A.Hamadi, S. Rahmani, and K. Al-Haddad, "A hybrid passive filter configuration for VAR control and harmonic compensation," IEEE Trans. Ind. Electron., vol. 57, no. 7, pp. 2419–2434, Jul. 2010.

[3] A.Varschavsky, J. Dixon, M. Rotella, and L. Moran, "Cascaded nine-level inverter for hybrid-series active power filter, using industrial controller," IEEE Trans. Ind. Electron., vol. 57, no. 8, pp. 2761–2767, Aug. 2010.

[4] A.Luo, X. Xu, L. Fang, H. Fang, J. Wu, and C. Wu, "Feedback– feedforward PI-type iterative learning control strategy for hybrid active power filter with injection circuit," IEEE Trans. Ind. Electron., vol. 57, no. 11, pp. 3767–3779, Nov. 2010.

[5] S. Rahmani, N. Mendalek, and K. Al-Haddad, "Experimental design of a nonlinear control technique for three-phase shunt active power filter," IEEE Trans. Ind. Electron., vol. 57, no. 10, pp. 3364–3375, Oct. 2010.

[6] B. Singh and J. Solanki, "An implementation of an adaptive control al- gorithm for a three-phase shunt active filter," IEEE Trans. Ind. Electron., vol. 56, no. 8, pp. 2811–2820, Aug. 2009.

[7] ABhattacharya and C. Chakraborty, "A shunt active power filter with enhanced performance using ANN-based predictive and adaptive con- trollers," IEEE Trans. Ind. Electron., vol. 58, no. 2, pp. 421–428, Feb. 2011.

[8] DGanthony and C. M. Bingham, "Integrated series active filter for aerospace flight control surface actuation," in Proc. EPE, 2007, pp. 1–9

[9] ELavopa, E. Summer, P. Zanchetta, C. Ladisa, and F. Cupertimo, "Real- time estimation of fundamental frequency and harmonics for active power filters applications in aircraft electrical systems," in Proc. EPE, 2007, pp. 4220–4229

[10] ELavopa, M. Summer, P. Zanchetta, C. Ladisa, and F. Cupertimo, "Real-time estimation of fundamental frequency and harmonics for active power filters applications in aircraft electrical systems," IEEE Trans. Ind. Electron., vol. 56, no. 8, pp. 2875–2884, Aug. 2009.

[11] M. Odavic, P. Zanchetta, and M. Summer, "A low switching frequency high bandwidth current control for active shunt power filter in aircrafts power networks," in Proc. IEEE IECON, 2007, pp. 1863–1868